ESD-TR-82-120

MTR-8354

AD A115059

FREQUENCY DEPENDENCE OF APATS ANTENNA GAIN

By

G. A. ROBERTSHAW

MARCH 1982

Prepared for

DEPUTY FOR SURVEILLANCE AND CONTROL SYSTEMS
ELECTRONIC SYSTEMS DIVISION
AIR FORCE SYSTEMS COMMAND
UNITED STATES AIR FORCE
Hanscom Air Force Base, Massachusetts

Approved for public release;
Distribution unlimited

Project No. 4290

Prepared by

THE MITRE CORPORATION
Bedford, Massachusetts

Contract No. F19628-81-C-0001

REVIEW AND APPROVAL

This technical report has been reviewed and is approved for publication.

Michael Zymaris /GS-13

MICHAEL ZYMARIS/GS-13
Project Officer

FOR THE COMMANDER

(Signature)
JAMES R. ARMSTRONG, Maj, USAF
Program Manager

UNCLASSIFIED

SECURITY CLASSIFICATION OF THIS PAGE *(When Data Entered)*

REPORT DOCUMENTATION PAGE		READ INSTRUCTIONS BEFORE COMPLETING FORM
1. REPORT NUMBER ESD-TR-82-120	2. GOVT ACCESSION NO. AD-A115059	3. RECIPIENT'S CATALOG NUMBER
4. TITLE *(and Subtitle)* FREQUENCY DEPENDENCE OF APATS ANTENNA GAIN		5. TYPE OF REPORT & PERIOD COVERED
		6. PERFORMING ORG. REPORT NUMBER MTR-8354
7. AUTHOR(s) G. A. ROBERTSHAW		8. CONTRACT OR GRANT NUMBER(s) F19628-81-C-0001
9. PERFORMING ORGANIZATION NAME AND ADDRESS The MITRE Corporation P. O. Box 208 Bedford, MA 01730		10. PROGRAM ELEMENT, PROJECT, TASK AREA & WORK UNIT NUMBERS Project No. 4290
11. CONTROLLING OFFICE NAME AND ADDRESS Deputy for Surveillance and Control Systems Electronic Systems Division, AFSC Hanscom Air Force Base, MA 01731		12. REPORT DATE MARCH 1982
		13. NUMBER OF PAGES 54
14. MONITORING AGENCY NAME & ADDRESS(*if different from Controlling Office*)		15. SECURITY CLASS. *(of this report)* UNCLASSIFIED
		15a. DECLASSIFICATION/DOWNGRADING SCHEDULE

16. DISTRIBUTION STATEMENT *(of this Report)*

Approved for public release; distribution unlimited

17. DISTRIBUTION STATEMENT *(of the abstract entered in Block 20, if different from Report)*

18. SUPPLEMENTARY NOTES

19 KEY WORDS *(Continue on reverse side if necessary and identify by block number)*

APATS
ARRAY DEGRADATION
DUAL FREQUENCY RECEPTION

20 ABSTRACT *(Continue on reverse side if necessary and identify by block number)*

If the APATS receiving array antenna is electronically steered by standard phase shifters at each element, the optimum gain for a signal arriving from a particular direction is dependent upon the frequency of the source. The APATS system requires simultaneous reception of two frequencies per re-entry vehicle, and optimum reception requires two sets of phase shifters per RV per polarization. This report examines the degradation of the array gain when one set of phase shifters is used for dual frequency reception. The gain of the array at the second, non-optimal, frequency is dependent upon frequency separation, array size and (over)

DD FORM 1 JAN 73 1473

UNCLASSIFIED

SECURITY CLASSIFICATION OF THIS PAGE *(When Data Entered)*

20. (Concluded)

illumination, and the direction cosines of the incident propagation vector with respect to the array axes. An array phase steering method which minimizes gain loss to one dB or less for typical cases is suggested.

ACKNOWLEDGMENTS

I wish to thank R.D. Preuss for his thorough review of the manuscript and valuable suggestions, and Mr. Bruce Rahn of ARIA Engineering for first suggesting the optimum beamsteering technique for dual link RV telemetry reception.

This report has been prepared by The MITRE Corporation under Project No. 4290. The contract is sponsored by the Electronic Systems Division, Air Force Systems Command, Hanscom Air Force Base, Massachusetts.

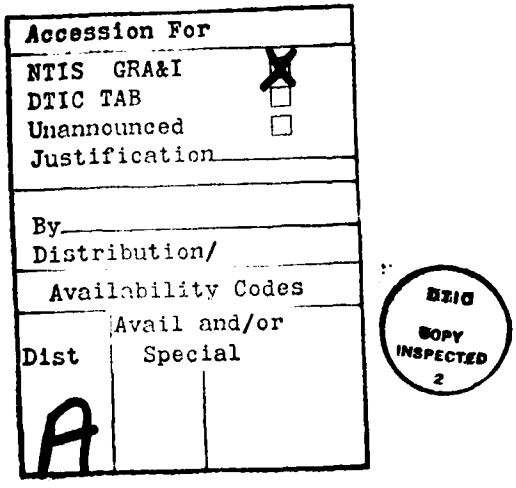

TABLE OF CONTENTS

LIST OF ILLUSTRATIONS

LIST OF TABLES

SECTION 1

SUMMARY

1.1 INTRODUCTION

If APATS employs a phase-steered array antenna, the feasibility of using a single set of phase shifters to simultaneously receive telemetry transmitted by one RV at two center frequencies, separated by up to 100 MHz, must be considered as an alternative to doubling the number of phase shifters for optimum reception. Dual frequency links are typically used to provide time diversity, since the second link, which is delayed, can recover data which may not survive real time transmission during the peak plasma loss or "blackout" period.

Unlike the broadband "lens fed" arrays, phase-steered arrays usually can only shift the RF phase of the incident field by 360° or less. The phase shifters are typically digitally switched delay line devices* which, for a 3-bit unit, provide any combination of 180°, 90° or 45° phase shifts by introducing line lengths of v/2f, v/4f and v/8f respectively, where f is the frequency and v is the velocity of the wave in the delay line. In contrast, a lens fed array provides time delays which insure absolute phase coherence at the output, rather than the modulo 360° phase coherence produced by conventional phase steering. Since the lens beamforming approach uses time delays to fully compensate for path length differences between the incident wavefront and receiving elements, its bandwidth is limited primarily by dispersion in the RF delay line (lens) material and receiving element bandwidth.

*M. I. Skolnik, Introduction to Radar Systems, New York: McGraw-Hill, 1980, pp. 286-288.

If a phased array is steered off its boresight by more than a few degrees*, the beam direction is frequency dependent. This follows since, for path length differences between the wavefront and array face of more than one RF wavelength, the time delays introduced by the 360° maximum phase shifters are insufficient to produce absolute coherence at the output.

1.2 RESULTS

Illustrative calculations, based on theoretical models discussed in detail in the following sections, have been performed for both linear and rectangular array models. A model which approximates the MITRE baseline antenna is a flat 3.13 m x 1.93 m rectangular array consisting of 1363 elements arranged in 29 rows and 47 columns. The array illumination is tapered to produce lower sidelobes. The more significant results for this model are summarized in Table 1. All gains are measured in dB and referenced to the optimum gain achievable by a set of phase shifters dedicated to the particular link frequency. A frequency separation of 58 MHz is the maximum anticipated[2] if existing frequency allocations are maintained, while a 100 MHz separation is the maximum possible within the APATS operational frequency band of 2.2 to 2.3 GHz. The phase steering is optimized when the beam is steered such that the losses at the two frequencies are equalized.† Thus, for the non-optimized examples, only one link suffers degradation, while for the optimized cases both links suffer a much smaller degradation.

Examination of Table 1 reveals that the worst optimized loss for a 58 MHz link separation is -0.58 dB, while if the full 100 MHz link separation is employed, each channel will lose 1.76 dB of gain.

---

* E.g., if "a" is aperture length in array azimuth plane, frequency dependence begins for $\emptyset > \sin^{-1}(\frac{\lambda}{a})$.

† Assumes both frequencies are equally important.

TABLE 1

Summary of Relative Gains for

APATS Baseline Array Antenna

OPTIMIZED?	FREQUENCY SEPARATION	GAIN REFERENCED TO OPTIMUM RECEPTION				
		ANGULAR COORDINATES OF SOURCE (FIG. 4)				
		ϕ=0; θ=0	ϕ=20;θ=0	ϕ=40;θ=0	ϕ=60;θ=0	ϕ=64.4,θ=-22*
NO	58 MHz	0 dB	-0.35	-1.26	-2.32	-2.38
NO	100 MHz	0	-1.06	-3.87	-7.35	-7.50
YES	58 MHz	0	-0.09	-0.31	-0.57	-0.58
YES	100 MHz	0	-0.26	-0.93	-1.71	-1.76

* Worst case.

Note that on antenna boresight ($\phi = 0$, $\theta = 0$) the array is broadband and that as the array azimuth angle off boresight, ϕ, is increased the losses become increasingly significant, as expected. Non-optimized losses are significantly larger; however, it must be remembered that only one channel is affected, since the array is optimally phased for one of the two frequencies. Loss splitting or dual frequency optimization does appear to have merit for the worst case examples in Table 1. These and other results are discussed further in later sections of this report; however, Table 1 does summarize the salient conclusions of this study.

If the optimized losses of up to -0.58 dB can be tolerated, only a single set of phase shifters per RV per polarization are necessary and a total of 10,904 fewer phase shifters in the context of this model are required for each APATS (1,363 x 4 RVs x 2 polarizations) array.

If optimized phase steering is employed, the conventional tracking algorithm must be slightly modified to correct systematic beam pointing errors associated with the difference between the beamforming (average) frequency and the (1 link) frequency used for tracking. The required corrections are derived in Appendix C, where it is also suggested that a coast mode using pre-stored and extrapolated trajectories be used during peak plasma loss for RV altitudes between 10 km and 30 km.

1.3 ORGANIZATION OF REPORT

The basic phase-steering concept and theory underlying the frequency dependence of the gain are formulated for a simple linear array in Section 2.1. The results of calculations predicated on this model are presented and discussed in Section 2.2. The one-

dimensional array results are instructive, since the relationships between the variables are simpler and more easily visualized for this case.

In Section 3.1 the theory introduced in Section 2.1 is applied to the somewhat more complicated two-dimensional array with a rectangular lattice of elements. Gain losses at the non-optimum frequency of the dual link are reported for a variety of incident wave vector directions for both uniformly illuminated and tapered arrays of two sizes in Section 3.2.

In Section 4, a method of phase steering which equalizes the losses in the two channels and optimizes the overall gain of the dual link is described. The APATS hardware savings possible if only one steered beam per RV per polarization is deemed adequate for dual frequency reception is also discussed.

In Appendix A the transformation of angular coordinates from the horizontal (local earth) coordinate system to the array-based coordinate system is mathematically described. Appendix B describes calculations pertaining to a cylindrically curved array and presents a brief set of results for a large tapered array. In Appendix C, RV tracking is discussed in the context of dual link optimized reception.

SECTION 2

LINEAR ARRAY

2.1 THEORY

For the simple ten element linear array illustrated in Figure 1, the path length difference from the wavefront, characterized by the propagation vector $\vec{k}$, to the nth array element position is given by,

$$\Delta P = n(\Delta x) \text{ SIN } \theta \qquad (1)$$

in which θ is the angle between $\vec{k}$ and a perpendicular to the array (boresight). Modulo 2π radians phase coherence is obtained for a propagation vector of magnitude,

$$|\vec{k}_1| = \frac{2\pi}{\lambda_1} = \frac{2\pi f_1}{c} \qquad (2)$$

if the nth array phase shifter introduces a phase shift of,

$$\phi_{f_1}(n) = \left[\frac{2\pi f_1 \; n(\Delta x) \; \text{SIN}\,\theta}{c}\right]_{\text{modulo } 2\pi} \qquad (3)$$

in which c is the speed of light. If the element spacing, Δx, is 6.67 cm, the transmitter frequency is 2.25 GHz, and θ is 50°, then a suitable phase shift configuration is as shown in Figure 2. This configuration is, of course, not unique since the "sawtooth" pattern may be moved laterally to generate other, equally valid configurations. It is the relative phase between the array's elements which is important, not the absolute phase reference value.

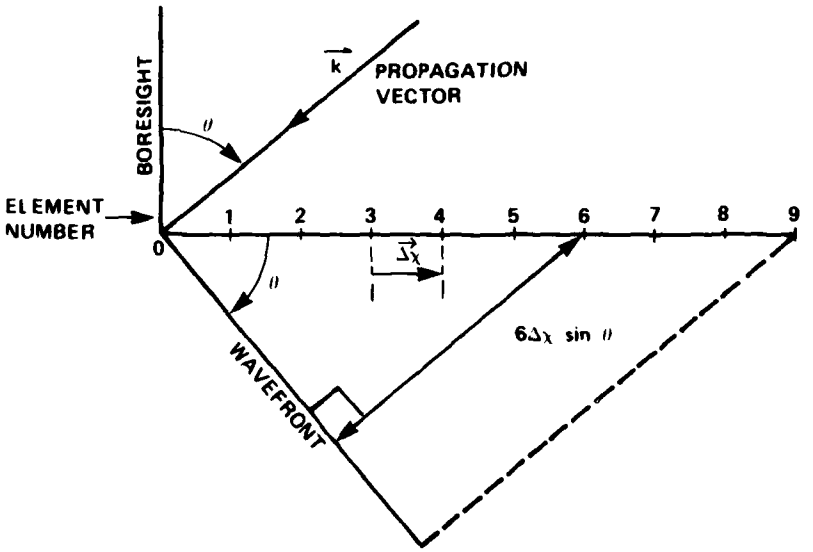

Figure 1. LINEAR ARRAY GEOMETRY

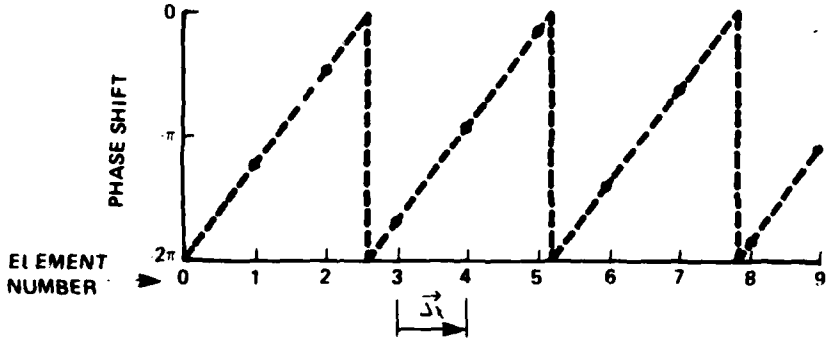

Δx = 6.67 cm, λ = 13.33 cm, θ = 50°

IA-61,889

Figure 2. PHASE SHIFTS FOR COHERENT (MODULO 2π) RECEPTION

With the phase shifters adjusted to satisfy Equation (3), imagine that a second wavefront characterized by a propagation vector $\vec{k}_2$ which is parallel to $\vec{k}_1$ is introduced, and that its phase is arbitrarily chosen to be identical to the first wavefront's phase at the origin (element 0). For array position "n" this wave has a phase given by,

$$\phi_{f_2}(n) = \vec{k}_{f_2} \cdot n\vec{\Delta x} = \frac{-2\pi f_2 \; n\Delta x \; \text{SIN} \; \theta}{c} \tag{4}$$

which, however, is phase shifted by the values which are set up for f_1. Thus, the net phase of the field at f_2, as seen by the array feed is,

$$\phi(n)_{\Delta f} = \left[\frac{2\pi\Delta f}{c} \; n(\Delta x) \; \text{SIN}\theta\right]_{\text{modulo } 2\pi} \tag{5}$$

in which,

$$\Delta f = f_1 - f_2 \tag{6}$$

Assuming $f_2 < f_1$, the wave at f_2 leads the one at f_1 by an amount of phase which changes in increments of,

$$\Delta\phi = \frac{2\pi(\Delta f)(\Delta x) \; \text{SIN} \; \theta}{c} \tag{7}$$

between ajacent array elements. The amplitude-phase diagram of Figure 3 shows that the element voltages associated with the (optimal) wavefront at f_1 are added coherently (in phase) for the phase shifter configuration of Equation (3), while the element voltages associated with the second, non-optimal, wavefront veer off in constant angular steps given by Equation (7) and give a net amplitude which is obviously less than optimal.

IA-61,901

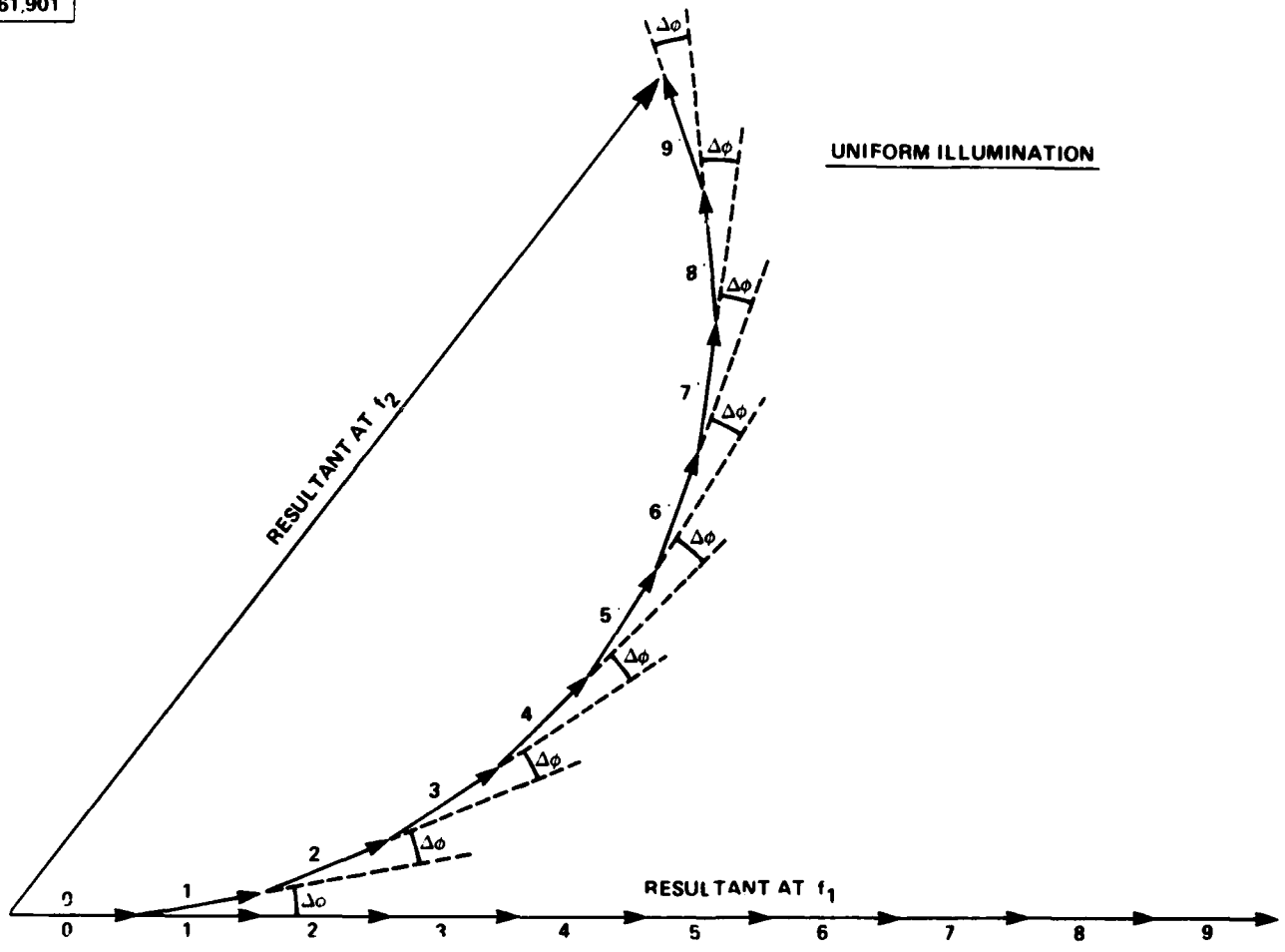

Figure 3. RELATIVE ARRAY OUTPUT VOLTAGE BY PHASOR ADDITION

Assuming that the phasor amplitudes are all equal, which corresponds to uniform illumination, the total voltage amplitude at the non-optimal frequency, f_2, relative to that at f_1 is given by,

$$\frac{V_{f_2}}{V_{f_1}} = V_{f_2,f_1} = \left| \frac{\sum_{n=0}^{N-1} e^{in\Delta\phi}}{\sum_{n=0}^{N-1} e^{o}} \right| \tag{8}$$

in which N is the total number of (evenly spaced) elements in the array. The truncated series of Equation (8) is a geometric progression which can be summed explicitly,

$$V_{f_2,f_1} = V_{\Delta f} = \left| \frac{\frac{1-e^{iN\Delta\phi}}{1-e^{i\Delta\phi}}}{N} \right| = \left| \left(e^{\frac{i(N-1)\Delta\phi}{2}} \right) \frac{\text{SIN } (\frac{N\Delta\phi}{2})}{N \text{ SIN } (\frac{\Delta\phi}{2})} \right| \tag{9}$$

$$= \left| \frac{\text{SIN } (\frac{N\Delta\phi}{2})}{N \text{ SIN } (\frac{\Delta\phi}{2})} \right|$$

The gain at f_2 relative to that at f_1 is,

$$g_R (\Delta\phi) = 20 \text{ LOG } \left| \frac{\text{SIN } (\frac{N\Delta\phi}{2})}{N \text{ SIN } (\frac{\Delta\phi}{2})} \right| \text{ (dB)} \tag{10}$$

If $\Delta\phi$ is very small compared to unity, Equation (10) reduces to the familiar result from diffraction theory,

$$g(x) = \frac{\text{SIN}^2 x}{x^2} \; ; \quad x = (\frac{N\Delta\phi}{2}) \tag{11}$$

This result is not surprising, and the wavefront at frequency f_2 is nearly equivalent to that from a second source at f_1 located at an angle off boresight,

$$\theta' = \text{SIN}^{-1} \left(\frac{f_2 \text{ SIN } \theta}{f_1}\right) \tag{12}$$

If the array element contributions to the total voltage are weighted, i.e., if aperture tapering is employed, Equation (8) must be replaced by a more general expression,

$$V_{f_2,f_1} = \left| \sum_{n=0}^{N-1} A(n)\ e^{in\Delta\phi} \Big/ \sum_{n=0}^{N-1} A(n) \right| \tag{13}$$

A typical expression for the weight function (unnormalized) or taper, A(n), is,

$$A(n) = 0.1 + \cos^2 \left[\frac{\pi\left[\frac{(N-1)}{2} - n\right]}{(N-1)}\right] \tag{14}$$

which describes an illumination which is symmetrical about the array center and decreases monotonically towards the ends of the array. The gain at the non-optimal frequency relative to that at the optimal frequency is given by,

$$g_R(\Delta\phi) = 20 \text{ LOG} \left| \frac{\sum_{n=0}^{N-1} A(n) e^{in\Delta\phi}}{\sum_{n=0}^{N-1} A(n)} \right| \text{ (dB)} \tag{15}$$

which can be evaluated numerically.

2.2 RESULTS

Relative gain calculations based on Equations (10) and (15) have been performed for a linear array consisting of 30 elements having a constant spacing of 6.67 cm, which is one-half a

wavelength at an RF of 2.25 GHz. This frequency is the center frequency of the 100 MHz wide band over which APATS must be operational. This model array can also represent azimuth or elevation beamforming for a two-dimensional array of the corresponding width or height.

The relative gain results for various combinations of scan angle and frequency separation are given in Table 2 and Table 3 for uniformly illuminated and tapered arrays, respectively. The weight function of Equation 14 was used to describe array taper. As expected, the loss increases monotonically with frequency separation and scan angle. The losses depend on Δf and are the same whether the array gain is optimized for f_1 or f_2. Furthermore, symmetry requires that the losses remain invariant under a sign reversal of the scan angle. Array tapering, which reduces antenna sidelobes and broadens the mainbeam, reduces frequency separation losses by more than 50% (in dB). Since the approximate maximum APATS azimuth scan angle (off boresight) is 60° and the maximum frequency separation is about 60 MHz, relative losses of $\sim$1.8 dB and $\sim$0.8 dB are anticipated at the non-optimal frequency for uniformly illuminated and tapered arrays respectively. More detailed and realistic estimates are computed for two-dimensional arrays in Section 3.2 and a three-dimensional (curved) array in Appendix B.

TABLE 2

Linear Array Calculations (Uniform Illumination)

θ \ Δf	50 MHz	60 MHz	70 MHz	80 MHz	90 MHz	100 MHz
50°	-0.95 dB	-1.38	-1.91	-2.53	-3.26	-4.11
55°	-1.09	-1.59	-2.20	-2.92	-3.77	-4.78
60°	-1.22	-1.79	-2.47	-3.29	-4.27	-5.43
65°	-1.34	-1.96	-2.72	-3.64	-4.73	-6.03
70°	-1.45	-2.12	-2.94	-3.94	-5.14	-6.58

TABLE 3

Linear Array Calculations (Tapered Illumination)

θ \ Δf	50 MHz	60 MHz	70 MHz	80 MHz	90 MHz	100 MHz
50°	-0.44 dB	-0.64	-0.87	-1.14	-1.45	-1.80
55°	-0.51	-0.73	-1.00	-1.31	-1.66	-2.06
60°	-0.57	-0.82	-1.12	-1.47	-1.86	-2.31
65°	-0.62	-0.90	-1.23	-1.61	-2.04	-2.53
70°	-0.67	-0.97	-1.32	-1.73	-2.20	-2.73

SECTION 3

RECTANGULAR ARRAY

3.1 THEORY

Although the linear array model provides valuable estimates of the power loss anticipated for a non-optimum frequency wavefront impinging on a phase steered array, a two-dimensional or planar array model, although more complicated, permits a more realistic and detailed assessment of the power losses which would be experienced by APATS.

Consider an incident plane wave, characterized by wavevector $\vec{k}_1$, incident upon a flat rectangular array, as illustrated in Figure 4. The elements are arranged in M rows and N columns which have separations of Δy and Δx respectively. The array origin is arbitrarily placed at the center of the element in the lower left-hand corner of the array. The position vectors of all of the elements with respect to this origin, are given by,

$$\vec{R}(n,m) = n(\Delta x)\,\hat{x} + m(\Delta y)\,\hat{y}$$

$$n = 0,\ 1,\ 2,\ \ldots,\ N-1 \qquad (16)$$

$$m = 0,\ 1,\ 2,\ \ldots,\ M-1$$

If the phase at the origin of the array is set to zero, the phase of the incident wave, $\vec{k}_1$, at element (n,m) is given by:

$$\phi_{k_1}(n,m) = \vec{k}_1 \cdot \vec{R}(n,m) = nk_{1x}\Delta x + mk_{1y}\Delta y \qquad (17)$$

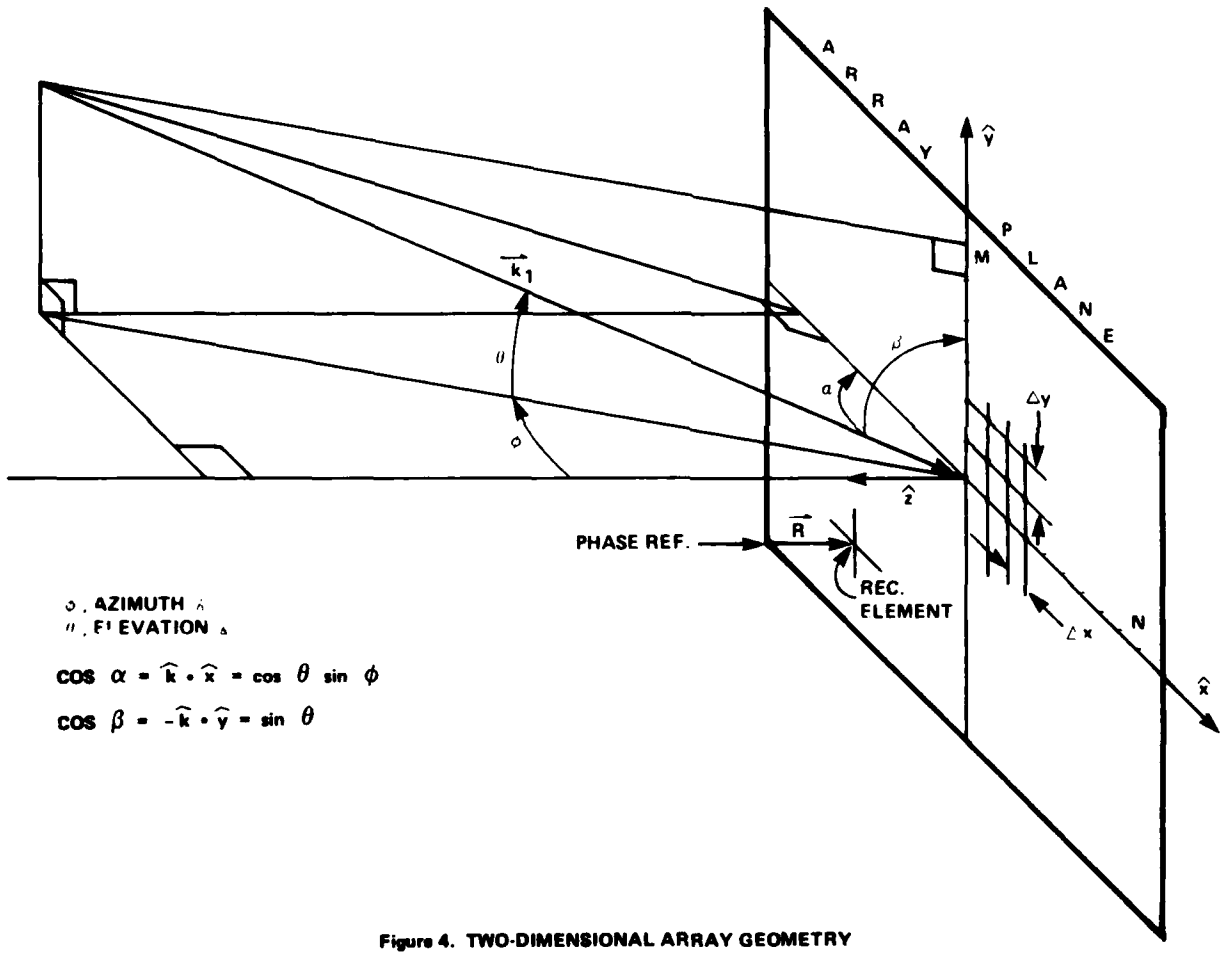

Figure 4. TWO-DIMENSIONAL ARRAY GEOMETRY

The components of $\vec{k}_1$ in the $\hat{x}$ and $\hat{y}$ directions can be expressed by the direction cosines, $\cos\alpha$ and $\cos\beta$ respectively, which in turn can be related to the azimuth and elevation angles as illustrated in Figure 4.

$$k_{1x} = |\vec{k}_1| \text{ COS } \alpha = |\vec{k}_1| \text{ COS } \theta \text{ SIN } \phi \tag{18a}$$

$$k_{1y} = -|\vec{k}_1| \text{ COS } \beta = -|\vec{k}_1| \text{ SIN } \theta \tag{18b}$$

The magnitude of the propagation vector is,

$$|\vec{k}_1| = \frac{2\pi}{\lambda_1} = \frac{2\pi f_1}{c} \tag{19}$$

To provide coherent (modulo 2π) reception for the wavefront at $\vec{k}_1$, the phase shifters of the array are set to negate the phase shifts of Equation (17):

$$\phi_{ps_{k_1}}(n,m) = [-\phi_{k_1}(n,m)]_{\text{modulo } 2\pi} \tag{20}$$

If a wavefront at $\vec{k}_2$, parallel to $\vec{k}_1$, is introduced, the net phase of the field due to $\vec{k}_2$ at the output of phase shifter (n,m), which has been set to provide optimum reinforcement at $\vec{k}_1$, is given by,

$$\Delta\phi_{k_2,k_1}(n,m) = [n\Delta\phi_{\hat{x}} + m\Delta\phi_{\hat{y}}]_{\text{modulo } 2\pi} \tag{21}$$

where,

$$\Delta\phi_{\hat{x}} = \frac{2\pi(\Delta f)\ (\Delta x)\ \text{COS } \theta \text{ SIN } \phi}{c} \tag{22a}$$

$$\Delta\phi_{\hat{y}} = \frac{-2\pi(\Delta f)\ (\Delta y)\ \text{SIN } \theta}{c} \tag{22b}$$

and,

$$\Delta f = f_2 - f_1 \tag{23}$$

If the array illumination is uniform, the voltage magnitude at the output of each phase shifter is equal and phasor addition, like that illustrated in Figure 3, is performed to calculate the relative amplitudes (voltages) of the components of the array output at f_1 and f_2:

$$\frac{V_{f_2}}{V_{f_1}} = V_{f_2,f_1} = \left| \frac{\sum_{n=0}^{N-1} \sum_{m=0}^{M-1} e^{i(n\Delta\phi_{\hat{x}} + m\Delta\phi_{\hat{y}})}}{\sum_{n=0}^{N-1} \sum_{m=0}^{M-1} e^{0}} \right|$$

$$= \frac{1}{NM} \left| \sum_{n=0}^{N-1} e^{in\Delta\phi_{\hat{x}}} \sum_{m=0}^{M-1} e^{im\Delta\phi_{\hat{y}}} \right| \tag{24}$$

The geometric progressions in Equations (24) may be summed, yielding the less cumbersome expression,

$$V_{f_2,f_1} = \left| \frac{\text{SIN}\left(\frac{N\Delta\phi_{\hat{x}}}{2}\right)}{N\ \text{SIN}\left(\frac{\Delta\phi_{\hat{x}}}{2}\right)} \ \frac{\text{SIN}\left(\frac{M\Delta\phi_{\hat{y}}}{2}\right)}{M\ \text{SIN}\left(\frac{\Delta\phi_{\hat{y}}}{2}\right)} \right| \tag{25}$$

which reduces to Equation (9) for the one-dimensional array if M=1 and Θ=0 as expected. The relative power is given by,

$$g_R(\vec{\Delta k}) = 20\ \text{LOG}(V_{f_2,f_1}) \quad \text{(dB)} \tag{26}$$

Aperture tapering is implemented by applying a suitable position dependent weight factor to each element output. Therefore, an amplitude function, A(n,m), is used to describe the amplitude of each component phasor so that the relative magnitude of the voltages at f_2 and f_1 is now,

$$V_{f_2,f_1} = \left| \frac{\sum_{n=0}^{N-1} \sum_{m=0}^{M-1} A(n,m)\, e^{i(n\Delta\hat{\phi}_x + m\Delta\hat{\phi}_y)}}{\sum_{n=0}^{N-1} \sum_{m=0}^{M-1} A(n,m)} \right| \tag{27}$$

A typical taper function has an amplitude which is a monotonically decreasing function of distance from the array center. Such a taper will reduce the sidelobe levels of the antenna power or gain pattern and also broaden the main lobe. The weight function used for the model calculations performed for this work is given by,

$$A(n,m) = 0.1 + \cos^2\left[\frac{\pi\left[(2n-N-1)^2 + (2m-M-1)^2\right]^{1/2}}{2\left[(N-1)^2 + (M-1)^2\right]^{1/2}}\right] \tag{28}$$

so that the overall complex weight function for beamsteering and tapering is,

$$A\left(\begin{smallmatrix} n,m \\ \phi,\theta \end{smallmatrix}\right) = A(n,m)e^{-i\left[\frac{n\, f_1 \Delta x \cos\theta \sin\phi - m\, f_1 \Delta y \sin\theta}{c}\right]} \tag{29}$$

for a beam in the (ϕ, θ) direction at f_1.

3.2 RESULTS

Planar array model calculations for the relative power of two parallel incident fields separated in frequency by Δf, with the array exactly phase steered to one frequency, were performed for four model rectangular arrays:

1) A uniformly illuminated 2.00 m x 1.33 m array comprised of 600 elements arranged in 20 rows and 30 columns (N=30, M=20).

2) Array (1) with tapered illumination as per Equation (28).

3) A uniformly illuminated 3.13 m x 1.93 m array comprised of 1363 elements arranged in 29 rows and 47 columns.

4) Array (3) with tapered illumination as per Equation (28).

Arrays 1 and 2 have an aperture of about 2.7 m^2 which is somewhat smaller than that of the existing ARIA dish antenna (3.5 m^2); however, arrays 3 and 4 have an aperture of 6.06 m^2 which is considerably larger than that of the dish in order to provide performance comparable to the dish antenna when the array is electronically steered approximately 60^o off boresight.

The relative antenna gain at the non-optimum frequency for array model (1) is given for selected azimuth ($\emptyset$) and elevation (θ) values in Tables 4 and 5 for frequency separations of 58 MHz and 100 MHz respectively. For two carriers allocated to one RV, 58 MHz is the largest anticipated frequency separation, while within the APATS operational bandwidth, 100 MHz represents the largest frequency separation possible. Note that for azimuth angles of 40^o or

TABLE 4

Small Rectangular Array Calculations

(Uniform Illumination)

(Δf = 58 MHz)

ϕ \ θ	0°	20°	40°	50°	60°
20°	-0.25 dB	-0.33	-0.54	-0.67	-0.78
30°	-0.54	-0.59	-0.71	-0.78	-0.86
40°	-0.90	-0.90	-0.92	-0.93	-0.94
50°	-1.29	-1.25	-1.14	-1.09	-1.04
60°	-1.66	-1.57	-1.36	-1.23	-1.13
70°	-1.97	-1.84	-1.53	-1.36	-1.20

TABLE 5

Small Rectangular Array Calculations

(Uniform Illumination)

(Δf = 100 MHz)

ϕ \ θ	0°	20°	40°	50°	60°
20°	-0.76 dB	-1.00	-1.64	-2.[illegible]	-2.41
30°	-1.65	-1.78	-2.15	-2.39	-2.63
40°	-2.80	-2.78	-2.79	-2.83	-2.89
50°	-4.11	-3.91	-3.50	-3.32	-3.18
60°	-5.43	-5.04	-4.19	-3.78	-3.45
70°	-6.58	-6.01	-4.78	-4.17	-3.67

less, the losses increase with elevation angle; however, for azimuth angles of 50° or greater, the losses decrease as the source elevation is increased. For APATS the locus of required look angles, $\emptyset$ and θ, with respect to the array coordinate system depends upon the field of view, which is specified in a horizontal coordinate system, and the tilt of the array boresight with respect to that horizontal system.* If the specified field of view is $\pm 60^{\circ}$ in a horizontal plane (azimuth) and from -15° to 45° in a vertical plane (elevation) and the array boresight is inclined 15° to optimize the antenna gain during the peak plasma loss period of re-entry, the locus of required scan directions in the array coordinate system is as shown in Figure 5. The worst losses for dual links occur for the points at the lower left and right corners of the envelope, that is $\emptyset = \pm 64.4^{\circ}$, $\theta = -22^{\circ}$. For these angular coordinates the relative gains at the non-optimum frequency are -1.68 dB and -5.40 dB for link separations of 58 MHz and 100 MHz, respectively.

Tables 6 and 7 present the relative losses for certain combinations of array azimuth and elevation at frequency separations of 58 MHz and 100 MHz respectively, for array model (2), which has a tapered aperture. The losses, in general, are significantly less than for the uniformly illuminated case considered previously. This result is not surprising since the tapered array is effectively smaller because the outer elements have a much smaller weight than the centrally situated elements. The greatest losses, which occur for scan coordinates of $\pm 64.4^{\circ}$ in array azimuth and -22° in array elevation, are -0.98 dB and -2.97 dB for frequency separations of 58 MHz and 100 MHz, respectively.

---

* See Appendix A for details.

IA-61,890

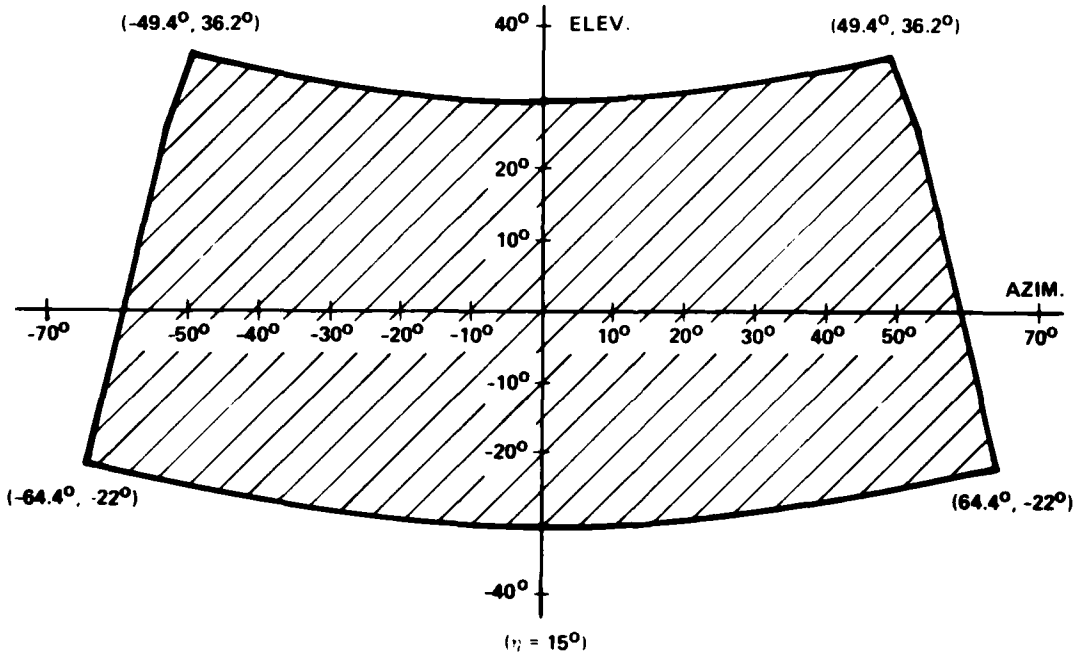

Figure 5. LOCUS OF REQUIRED SCAN ANGLES REFERENCED TO ARRAY COORDINATE SYSTEM

TABLE 6

Small Rectangular Array Calculations

(Tapered Illumination)

(Δf = 58 MHz)

ϕ \ θ	0°	20°	40°	60°
20°	-0.14 dB	-0.22	-0.40	-0.60
40°	-0.51	-0.54	-0.61	-0.70
60°	-0.94	-0.91	-0.86	-0.80

TABLE 7

Small Rectangular Array Calculations

(Tapered Illumination)

(Δf = 100 MHz)

ϕ \ θ	0°	20°	40°	60°
20°	-0.43 dB	-0.64	-1.19	-1.84
40°	-1.54	-1.62	-1.84	-2.11
60°	-2.85	-2.77	-2.59	-2.42

The larger aperture array models (3) and (4) on page 20 should be far more sensitive to carrier frequency separation of dual link sources than the previous models, since the main beamwidths of the larger arrays are significantly narrower. Indeed, the results of calculations, which appear in Tables 8 through 11, confirm this expectation. For the uniformly illuminated array and a frequency separation of 100 MHz, the relative gain at the non-optimum frequency falls off precipitously as the beam direction increases in azimuth for low elevation values (Table 9). This trend is far less pronounced for the 58 MHz separation as indicated in Table 8. Once again, the greatest losses will occur at the lower corners of the $\emptyset - \theta$ envelope of Figure 5, for which the non-optimum frequency is received with 4.32 dB and 17.8 dB less gain for frequency separations of 58 MHz and 100 MHz, respectively.

When the large aperture array illumination is tapered, the losses are greatly ameliorated as indicated by the results which appear in Tables 10 and 11. The worst case APATS scan angles of $\pm 64.4^{\circ}$ in azimuth and -22° in elevation produce losses of -2.38 dB and -7.50 dB for frequency separations of 58 MHz and 100 MHz, respectively.

Thus, larger arrays will produce a higher gain beam for a particular source frequency, and discriminate more effectively against a second link at a different (non-optimum) frequency when the source is off array boresight.

TABLE 8

Large Rectangular Array Calculations

(Uniform Illumination)

(Δf = 58 MHz)

ϕ \ θ	0°	20°	40°	50°	60°
20°	-0.62 dB	-0.78	-1.20	-1.46	-1.70
30°	-1.35	-1.42	-1.62	-1.75	-1.88
40°	-2.28	-2.24	-2.15	-2.12	-2.10
50°	-3.33	-3.14	-2.73	-2.51	-2.33
60°	-4.36	-4.03	-3.28	-2.89	-2.56
70°	-5.25	-4.79	-3.75	-3.21	-2.74

TABLE 9

Large Rectangular Array Calculations

(Uniform Illumination)

(Δf = 100 MHz)

ϕ \ θ	0°	20°	40°	50°	60°
20°	-1.91 dB	-2.38	-3.70	-4.58	-5.48
30°	-4.32	-4.47	-5.02	-5.48	-6.01
40°	-7.80	-7.40	-6.78	-6.65	-6.69
50°	-12.62	-11.23	-8.85	-7.98	-7.44
60°	-19.66	-16.09	-11.06	-9.33	-8.17
70°	-34.47	-22.27	-13.13	-10.50	-8.78

TABLE 10

Large Rectangular Array Calculations

(Tapered Illumination)

(Δf = 58 MHz)

ϕ \ θ	0°	20°	40°	60°
20°	-0.35 dB	-0.50	-0.89	-1.34
40°	-1.26	-1.30	-1.42	-1.56
60°	-2.32	-2.23	-2.02	-1.82

TABLE 11

Large Rectangular Array Calculations

(Tapered Illumination)

(Δf = 100 MHz)

ϕ \ θ	0°	20°	40°	60°
20°	-1.06 dB	-1.50	-2.70	-4.19
40°	-3.87	-3.97	-4.31	-4.86
60°	-7.35	-6.99	-6.23	-5.64

SECTION 4

GAIN OPTIMIZATION

In the preceding two sections, which considered linear and rectangular arrays, it was always assumed that the array was phase steered to one of the two carrier frequencies of the source. The relative gain at the second frequency was then derived. As has been suggested, it should be possible to phase steer the array between the two frequencies so that both links suffer the same loss. The advantage gained by this technique is evident from Figure 6, which displays relative gain versus azimuth angle (θ=0) for the large rectangular array with uniform illumination. If the link separation is 100 MHz and one channel is optimized, the remaining channel degrades rapidly as the array is steered off boresight. If, however, the array phase shifts are adjusted to split the frequency separation to 50 MHz per channel, the (equal) degradation of the channels is relatively mild as the array is steered off boresight. To equalize the gain of the array for the two sources described by wave vectors,

$$\vec{k}_1 = \frac{2\pi f_1}{c}\hat{k} \quad , \quad \vec{k}_2 = \frac{2\pi f_2}{c}\hat{k} \tag{30}$$

The phase shift of element (n,m) is adjusted to the average value of the phases required for wavefronts $\vec{k}_1$ and $\vec{k}_2$ alone,

$$\phi_{ps_{k_{AVE}}}(n,m) = \left[\frac{-\pi(f_1 + f_2)\,\hat{k}\cdot\vec{R}\,(n,m)}{c}\right] \text{ modulo } 2\pi \tag{31}$$

in contrast to the result of Equation (20) which optimizes the phase shifts for $\vec{k}_1$. In Table 12 the relative link gains for optimized

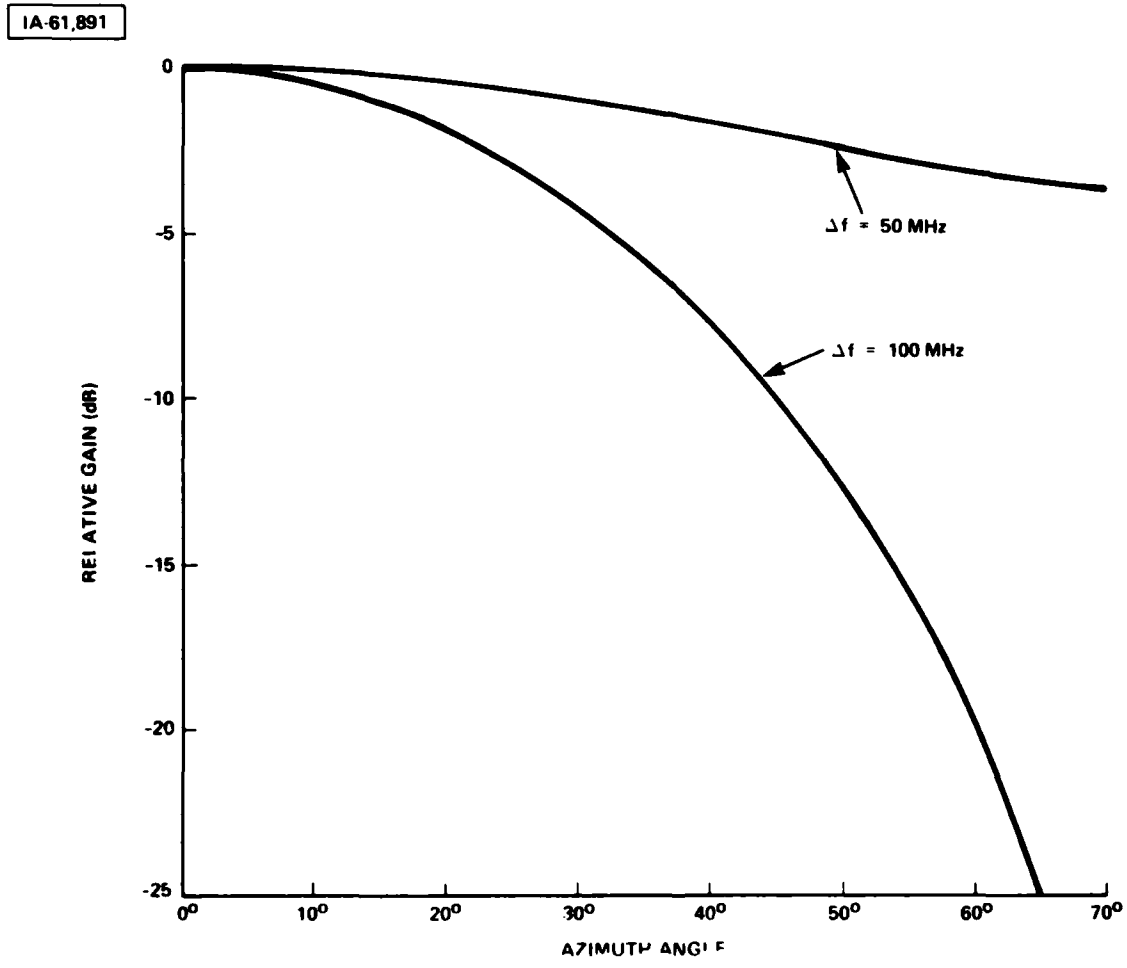

Figure 6 RELATIVE GAIN VERSUS AZIMUTH ANGLE FOR 47 x 29 ARRAY (ELEV = 0 UNIFORM ILLUMINATION)

TABLE 12

Relative Link Gains for Single Frequency
and Dual Frequency Optimized Phased Arrays
Steered to Maximum Required Angle off Boresight
(Array Azimuth = $\pm 64.4^{o}$, Array Elevation = -22^{o})

NO.	OPTIMIZED?	ILLUMINATION	ARRAY	Δf(MHz)	RELATIVE GAIN	
					LINK 1	LINK 2
1	NO	UNIFORM	30x20	58	0 dB	-1.68 dB
2	YES	↓	↓	↓	-0.41	-0.41
3	NO	↓	↓	100	0	-5.40
4	YES	↓	↓	↓	-1.24	-1.24
5	NO	TAPERED	↓	58	0	-0.98
6	YES	↓	↓	↓	-0.24	-0.24
7	NO	↓	↓	100	0	-2.97
8	YES	↓	↓	↓	-0.72	-0.72
9	NO	UNIFORM	47x29	58	0	-4.32
10	YES	↓	↓	↓	-1.01	-1.01
11	NO	↓	↓	100	0	-17.84
12	YES	↓	↓	↓	-3.13	-3.13
13	NO	TAPERED	↓	58	0	-2.38
14	YES	↓	↓	↓	-0.58	-0.58
15	NO	↓	↓	100	0	-7.50
16	YES	↓	↓	↓	-1.76	-1.76

TABLE 13

Comparison of Hardware for APATS
With 1 Steerable Beam Per RV Per Polarization
Vs. 2 Steerable Beams Per RV Per Polarization

HARDWARE ITEM	1 BEAM PER POL. PER RV	2 BEAMS PER POL. PER RV
ARRAY ELEMENTS	1,363	1,363
LOW NOISE AMPLIFIERS	2,726	2,726
PHASE SHIFTERS	10,904	21,808
COMBINERS*	8	16

* Without Monopulse Tracking

beamsteering are compared with previous results. The worst losses are sustained for case No. 12, for which the gain is down by 3.13 dB for each channel relative to the optimum single frequency gain. Since it is likely that the APATS antenna will be approximately 6 m^2 in aperture and will be tapered, case 14, which has 0.58 dB of loss per channel, is the most realistic array model. Indeed, it may be acceptable to steer the array to one frequency and incur a 2.38 dB loss in the non-optimum channel as indicated by case 13, if it is desired that one signal be as strong as possible.

If both signals must be received with optimum strength, independent sets of phase shifters and separate combining networks must be employed. A breakdown of the APATS hardware requirements for both single beam and dual beam (per RV per polarization) reception appears in Table 13. The specific figures apply to the large array comprised by 29 rows and 47 columns of receiving elements. Two low noise amplifiers are necessary per element--one for each polarization. To obtain optimum performance at each frequency for 4 dual link RVs would require 10,904 additional phase shifters and 8 additional combining networks. If each link is provided with tracking capability, the 2 beam per RV per polarization design incurs additional hardware requirements which will be dependent upon the type of tracking used.

There is obviously an incentive to keep the APATS system as simple as possible while not seriously jeopardizing its capability. This report has investigated and compared two beamsteering options (optimized and non-optimized single beam) and their impact on antenna gain. It is hoped that this information will be of assistance.

APPENDIX A

TRANSFORMATION FROM HORIZONTAL TO ARRAY ANGULAR COORDINATES

In this appendix the transformation from angular coordinates in the horizontal reference frame (ϕ_h, θ_h) to angular coordinates in the array frame (ϕ, θ) is mathematically described.

The horizontal reference frame is simply the local earth coordinate system in which azimuth and elevation retain their conventional meanings. In cartesian coordinates the $\hat{y}$ direction is taken to be straight up, while the $\hat{z}$ direction is defined as horizontal and perpendicular to the array longitudinal axis. The $\hat{x}$ direction then lies along the array longitudinal axis, which is assumed to be horizontal, with direction given by,

$$\hat{x} = \hat{y} \times \hat{z} \tag{32}$$

as required for a right-handed coordinate system. If a unit vector $\hat{k}$ has azimuth and elevation given by ϕ_h and θ_h respectively, as shown in Figure 7, its cartesian coordinates are given by,

$$\hat{k} = \cos\theta_h \sin\phi_h \hat{x} + \sin\theta_h \hat{y} + \cos\theta_h \cos\phi_h \hat{z} \tag{33}$$

The array coordinate system is obtained by rotating the horizontal coordinate system by η degrees about the $\hat{x}$ or longitudinal array axis. The angle η is the elevation of the array boresight as measured in the horizontal frame, as illustrated in Figure 7. The transformation equations are, in matrix form,

$$\hat{k}' = \begin{pmatrix} k'_x \\ k'_y \\ k'_z \end{pmatrix} = \begin{pmatrix} 1 & 0 & 0 \\ 0 & \cos\eta & -\sin\eta \\ 0 & \sin\eta & \cos\eta \end{pmatrix} \begin{pmatrix} k_x \\ k_y \\ k_z \end{pmatrix} \tag{34}$$

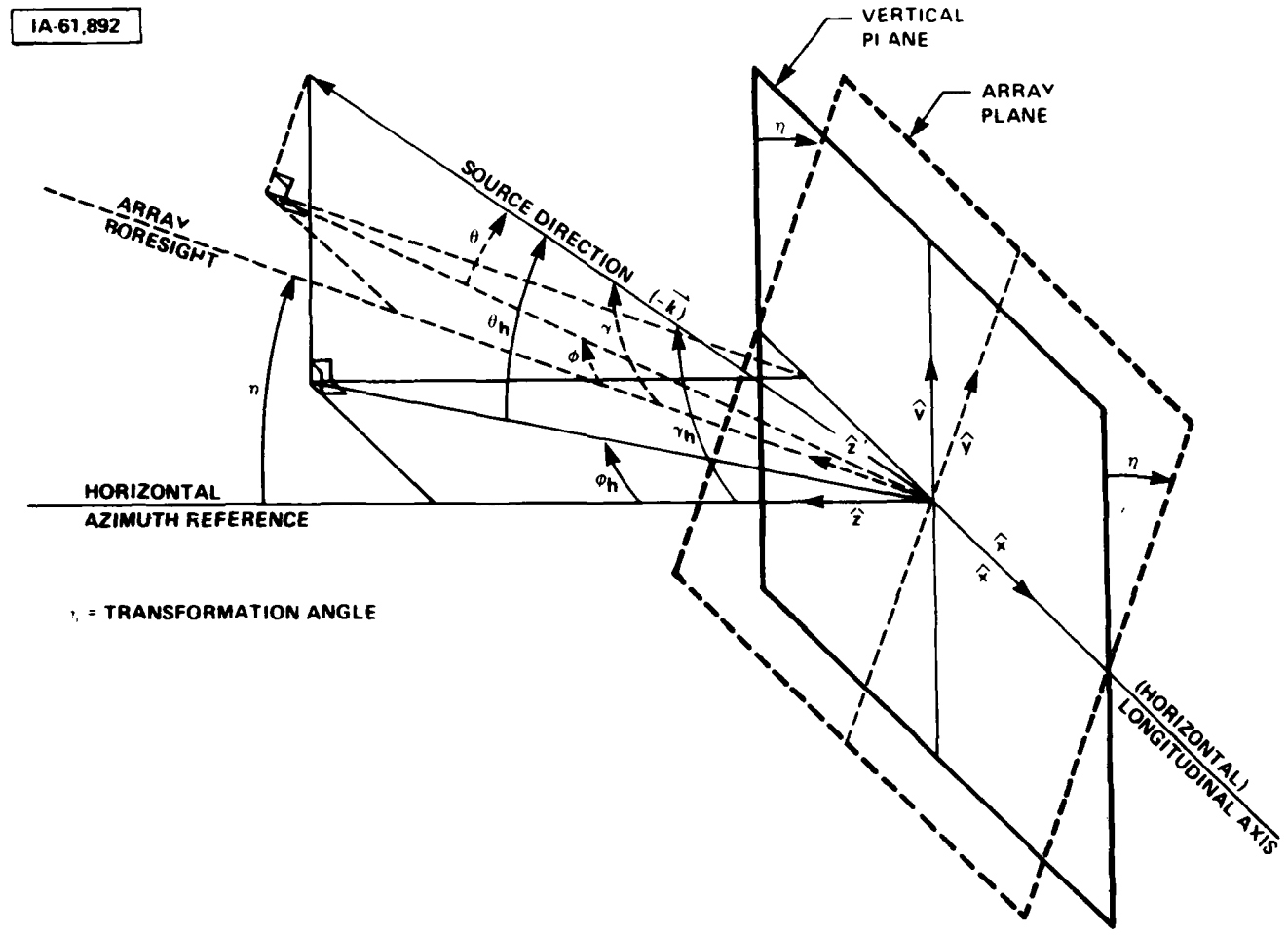

Figure 7. ELEVATION AND AZIMUTH FOR HORIZONTAL AND ARRAY COORDINATE SYSTEMS

in which primed coordinates designate quantities measured in the array system. The desired angular coordinates of $\hat{k}'$ can then be obtained from,

$$\phi = \text{TAN}^{-1}\left(\frac{k'_x}{k'_z}\right) \tag{35}$$

$$\theta = \text{TAN}^{-1}\left(\frac{k'_y}{\left[(k'_x)^2 + (k'_z)^2\right]^{1/2}}\right) \tag{36}$$

The angle of $\hat{k}'$ off array boresight is straightforwardly obtained from,

$$\gamma = \text{COS}^{-1}\left[\hat{k}' \cdot \hat{z}'\right] = \text{COS}^{-1}\left[\text{COS}\,\theta\,\text{COS}\,\phi\right] \tag{37}$$

or in terms of ϕ_h, θ_h and η:

$$\gamma = \text{COS}^{-1}\left[\text{SIN}\,\eta\,\text{SIN}\,\theta_h + \text{COS}\,\eta\,\text{COS}\,\theta_h\,\text{COS}\,\phi_h\right] \tag{38}$$

Array angular coordinates, ϕ, θ, and γ, are given in Table 14 for selected combinations of azimuth (ϕ_h) and elevation (θ_h) in the horizontal coordinate system, for $\eta = 15^\circ$ as recommended in the MITRE APATS baseline model.

The above transformation was also used to map the specified APATS field of view boundary ($-60^\circ < \phi_h < 60^\circ$, $-15^\circ < \theta_h < 45^\circ$) into the array coordinate system as illustrated by Figure 5.

TABLE 14

Array Angular Coordinates for Selected Combinations of Azimuth and Elevation in Horizontal Reference Frame

θ_h \ ϕ_h	0°	10°	20°	30°	40°	50°	60°
60°	0° ϕ	7.0	14.1	21.2	28.4	35.6	42.9
	45° θ	45.1	45.6	46.4	47.5	48.8	50.5
	45° γ	45.5	47.3	50.0	53.5	57.6	62.2
45°	0	8.1	16.3	24.5	32.7	41.0	49.4
	30	30.1	30.7	31.6	32.8	34.4	36.2
	30	31.1	34.4	39.2	45.0	51.5	58.3
30°	0	8.9	17.9	26.8	35.8	44.8	53.8
	15	15.2	15.8	16.7	18.1	19.8	21.7
	15	17.5	23.7	31.3	39.6	48.1	56.7
15°	0	9.6	19.2	28.8	38.4	47.9	57.4
	0	0.2	0.8	1.9	3.3	5.1	7.1
	0	9.6	19.3	28.9	38.5	48.1	57.7
0°	0	10.3	20.6	30.8	40.9	50.9	60.8
	-15	-14.7	-14.0	-12.9	-11.4	-9.5	-7.4
	15	17.9	24.8	33.2	42.2	51.6	61.1
-15°	0	11.1	22.1	33.0	43.7	54.2	64.4
	-30	-29.7	-29.0	-27.8	-26.2	-24.2	-22.0
	30	31.5	35.9	42.1	49.6	57.8	66.4

APPENDIX B

CALCULATIONS FOR CYLINDRICAL ARRAY

It is likely that the APATS array will be conformal, i.e., the array will follow the cylindrical contour of the ARIA fuselage. To investigate the effects of array conformality, in the context of beamsteering frequency sensitivity, the rectangular array model can be readily generalized to a three-dimensional cylindrically curved array, by introducing an axis of curvature parallel to $\hat{x}$ and in the x-z plane a distance R behind the array, as illustrated in Figure 8. The elements are arranged in M rows parallel to the cylinder axis and separated by segments of length Δc measured along the cylinder surface. Each row is comprised of N elements with spacings of Δx. Element position vectors, relative to the origin illustrated in Figure 8, are generated by,

$$R(n,m) = -n\Delta x\,\hat{x} + R\,\text{SIN}\,[(M-1-2m)\alpha]\,\hat{y} + R\,[\text{COS}[(M-1-2m)\alpha]-1]\,\hat{z} \qquad (39)$$

$$n = 0, 1, 2, \ldots, N-1$$
$$m = 0, 1, 2, \ldots, M-1$$

in which,

$$\alpha = \frac{\Delta c}{2R} \quad \text{RADIANS} \qquad (40)$$

The difference in the incident wave vector due to a shift in source frequency, Δf, is represented by,

$$\Delta k = \frac{2\pi\Delta f}{c}\,[\text{COS}\,\theta\,\text{SIN}\,\phi\,\hat{x} + \text{SIN}\,\theta\,\hat{y} + \text{COS}\,\theta\,\text{COS}\,\phi\,\hat{z}] \qquad (41)$$

IA-61,903

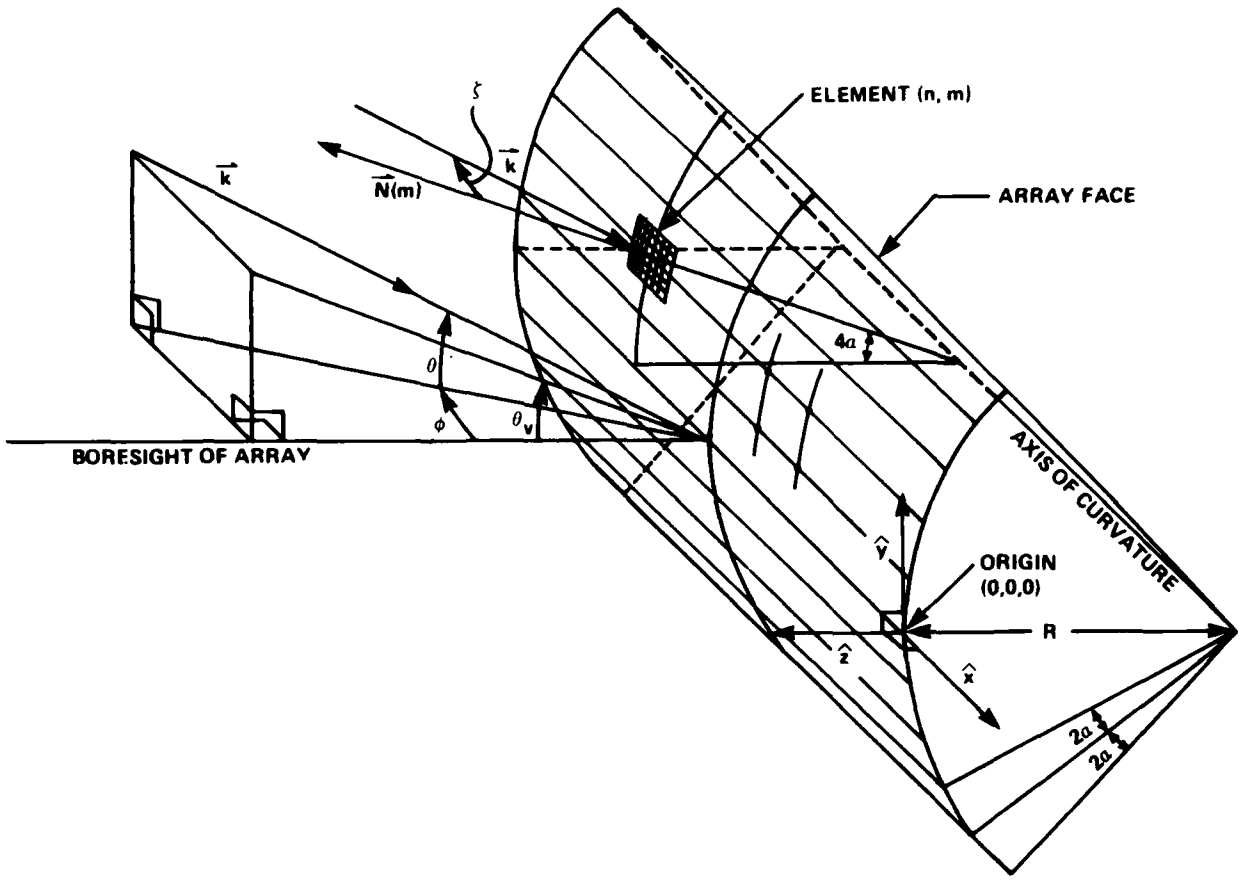

Figure 8. CYLINDRICAL ARRAY GEOMETRY

in which c is the speed of light, and θ and ϕ are the elevation and azimuth angles of $\vec{k}$ in the array coordinate system.

If the array elements and incident field are polarization matched, as will be assumed for this simple model, the voltage output of an element is assumed to be proportional to the square root of the projection of the element area on the plane perpendicular to $\vec{k}$. This assumption is made in lieu of an "imbedded" element pattern to account, in an admittedly crude fashion, for geometrical effects arising from array curvature. For the flat or linear array models, element pattern factors were identical for all elements* and could therefore be factored out of the array voltage summations and cancelled. To mathematically formulate the above assumption, it is convenient to introduce a unit vector $\hat{N}(m)$ which is normal to the elements in the m th row (rows are counted from the top of the array),

$$\hat{N}(m) = \text{SIN}\,[(M-1-2m)\alpha]\,\hat{y} + \text{COS}\,[(M-1-2m)\alpha]\,\hat{z} \qquad (42)$$

The projection of a given element's area on the incident wavefront is proportional to the cosine of the angle, ζ, between $\vec{k}$ and $\hat{N}$ as shown in Figure 8. The voltage induced in this element is assumed to be proportional to the square root of the projected area,

$$V(m) \propto (\cos\zeta)^{1/2} = [\hat{k} \cdot \hat{N}(m)]^{1/2} \qquad (43)$$

$$= [\text{SIN}\,\theta\,\text{SIN}[(M-1-2m)\alpha] + \text{COS}\,\theta\,\text{COS}\,\phi\,\text{COS}\,[(M-1-2m)\alpha]]^{1/2}$$

In addition to the amplitude variation expressed by Equation (43), a deliberate taper factor, A(n,m), may be introduced to produce lower sidelobes. The voltage at f_2 relative to f_1, if the array is optimized for f_1, is given by,

---

* If edge effects are neglected.

$$V_{f_2,f_1} = \frac{V_{f_2}}{V_{f_1}} = \left| \frac{\sum_{n=0}^{N-1} \sum_{m=0}^{M-1} (\hat{k}\cdot\hat{N}(m))\ A(n,m) e^{i\Delta\vec{k}\cdot\vec{R}(n,m)}}{\sum_{n=0}^{N-1} \sum_{m=0}^{M-1} (\hat{k}\cdot\hat{N}(m))\ A(n,m)} \right| \qquad (44)$$

which is analogous to Equation (27) which expressed the relative voltage for the flat rectangular array. The power loss at f_2 referenced to 0 dB at f_1 is given again by Equation (26),

$$g_R(\Delta\vec{k}) = 20\ \mathrm{LOG}\left(V_{f_2,f_1}\right)\ \mathrm{(dB)} \qquad (26)$$

Numerical calculations have been performed for a model cylindrical array having 29 rows and 47 columns with $\Delta x = \Delta C = 6.67$ cm. The array surface area is 6.06 m^2 while the area projected onto a plane perpendicular to the array boresight is 5.48 m^2. The radius of curvature, 1.85 m, corresponds approximately to the radius of the upper half cylinder of the ARIA fuselage.

The results of the relative gain calculations for this model appear in Tables 15 and 16 for frequency separations of 58 MHz and 100 MHz respectively. For these calculations, the taper function of Equation (28) was employed. Since the curved array can be imagined as simply the large rectangular array (Model 4) of Section 3.2 wrapped around a cylinder of 2.85 m radius with its longitudinal axis parallel to the cylinder axis, it is interesting to compare Tables 15 and 16 with Tables 10 and 11 respectively. As anticipated, in most cases the results are nearly equal, since the array curvature is not great; however, for large source elevation angles, losses for the cylindrical array are significantly less. This last observation is a consequence of array shadowing associated with curvature as discussed below.

TABLE 15

Large Cylindrical Array

(Tapered Illumination)

(Δf = 58 MHz)

ϕ \ θ	0°	20°	40°	60°
20°	-0.38 dB	-0.50	-0.81	-0.99
40°	-1.28	-1.29	-1.32	-1.10_{27}
60°	-2.32	-2.21	-1.87	-1.16_{23}

TABLE 16

Large Cylindrical Array

(Tapered Illumination)

(Δf = 100 MHz)

ϕ \ θ	0°	20°	40°	60°
20°	-1.13	-1.50	-2.44	-3.03
40°	-3.92	-3.95	-4.01	-3.33_{27}
60°	-7.38	-6.94	-5.75	-3.51_{23}

The array elevation angle of $\vec{k}$ projected onto a plane perpendicular to the axis of curvature is,

$$\theta_v = \text{TAN}^{-1}\left(\frac{\text{TAN } \theta}{\text{COS } \phi}\right) \tag{45}$$

while the angle between the normal to the m th row of elements and the boresight is given by,

$$\theta_N = (M-1-2m)\alpha = \frac{(M-1-2m)\Delta c}{2R} \tag{46}$$

If,

$$\theta_v - \theta_N \geq 90^\circ \tag{47}$$

the m th row of elements is geometrically shadowed by the bulge of the array and does not participate in beamforming. Diffraction around the array is neglected. For certain combinations of source angular coordinates in Tables 15 and 16, shadowing had to be taken into account, and in such cases the number of element rows which participate in reception is noted in the lower right-hand corner of the respective box. The total number of rows is 29. Since shadowing reduces the effective aperture of the array, frequency sensitivity is diminished and the losses at the non-optimum frequency are consequently less.

Worst case relative losses for the cylindrical array model occur for the array angular coordinates $\phi = \pm 64.4^\circ$, $\theta = -22^\circ$ and are -2.36 dB for 58 MHz separation and -7.42 dB for the 100 MHz separation. Equalizing the losses in the two channels by average phase steering yields the optimized losses of -0.58 dB and -1.74 dB for 58 MHz separation and 100 MHz separation respectively. These values are very close to those obtained for the large rectangular (flat) tapered array (see Table 12).

APPENDIX C

TRACKING WITH AN OPTIMIZED BEAM

As discussed in Section 4, the array gain for a dual link RV can be optimized by steering a beam in the direction of the RV using phase commands predicated upon reception of the average of the two link frequencies. This technique will require modification of conventional tracking strategies as is discussed below.

Assume that a dual link RV has carrier frequencies centered at f_1 and f_2 and that these transmissions arrive from a direction characterized by direction cosine angles α and β with respect to the array $\hat{x}$ and $\hat{y}$ axes, respectively. The tracking objective is to point the beam formed at the average frequency, $(f_1 + f_2)/2$, in the direction (α, β) at all times as required by the gain optimization method described earlier. Sequential lobe tracking, for example, points the array beam along a sequence of slightly different directions (1°~2°) and processes the signal strength measurements thereby collected to obtain an accurate estimate of the beam position for which the received power at the frequency used for tracking is maximized. For a dual link RV, it is likely that only one frequency will be employed for tracking measurements, and, therefore, if corrective action is not taken, the tracking algorithm will optimize reception at the tracking frequency and defeat the objective of balanced reception and optimized gain for both links.

To illustrate the above considerations, imagine that a beam formed using phase commands based upon the average frequency is steered in the (α', β') direction, close to the true RV direction (α, β). If the signal at f_1 is used for tracking, the normalized gain at f_1 is given by, if projected aperture dependence is neglected,

$$g(f_1) = 20 \text{ LOG} \left| \frac{\text{SIN } (\frac{N\Delta\phi_x}{2}) \text{ SIN } (\frac{M\Delta\phi_y}{2})}{N \text{ SIN } (\frac{\Delta\phi_x}{2}) \text{ M SIN } (\frac{\Delta\phi_y}{2})} \right| \tag{48}$$

$$\Delta\phi_x = \frac{2\pi\Delta x}{c} \left[f_1 \cos\alpha - \frac{(f_1 + f_2)}{2} \cos\alpha' \right] \tag{49a}$$

$$\Delta\phi_y = \frac{2\pi\Delta y}{c} \left[f_1 \cos\beta - \frac{(f_1 + f_2)}{2} \cos\beta' \right] \tag{49b}$$

which is applicable for an array with M rows spaced by increments of Δy and N columns spaced by increments of Δx. Clearly, the gain at f_1 is maximized as $\Delta\phi x$ and $\Delta\phi y$ approach zero, and, if beamforming were performed at f_1, tracking would cause the beam direction to approach the true RV direction:

$$\alpha' \longrightarrow \alpha, \ \beta' \longrightarrow \beta \tag{50}$$

However, since beamforming is based on the average frequency, the maximum gain is realized when,

$$\Delta\phi x = 0 \quad \text{OR,} \quad f_1 \cos\alpha = \frac{f_1+f_2}{2} \cos\alpha' = \frac{f_1+f_2}{2} \cos(\alpha + \Delta\alpha) \tag{50a}$$

$$\Delta\phi y = 0 \quad \text{OR,} \quad f_1 \cos\beta = \frac{f_1+f_2}{2} \cos\beta' = \frac{f_1+f_2}{2} \cos(\beta + \Delta\beta) \tag{50b}$$

and if,

$$\Delta\alpha \ll 1, \quad \Delta\beta \ll 1 \tag{51}$$

$$\alpha' = \alpha + \Delta\alpha \cong \alpha + \left(\frac{f_1 - f_2}{f_1 + f_2} \right) \cot\alpha \quad \text{(RADIANS)} \tag{52a}$$

$$\beta' = \beta + \Delta\beta \cong \beta + \left(\frac{f_1 - f_2}{f_1 + f_2}\right) \text{COT}\ \beta \quad \text{(RADIANS)} \tag{52b}$$

which result indicates that the average (optimized) frequency beam will be offset by angular increments $\Delta\alpha$ and $\Delta\beta$ from the true RV position if tracking is performed at f_1. Gain optimization for both links requires that the optimized beam be directed at the true RV position, so it is necessary to introduce the angular corrections,

$$\alpha_c = -\Delta\alpha \cong \left(\frac{f_2 - f_1}{f_1 + f_2}\right) \text{COT}\ \alpha' \tag{53a}$$

$$\beta_c = -\Delta\beta \cong \left(\frac{f_2 - f_1}{f_1 + f_2}\right) \text{COT}\ \beta' \tag{53b}$$

in which α' and β' have been substituted for α and β with negligible error, to maintain an optimized track. The tracking computer can implement the necessary corrections after receiving the updated tracking coordinates; however, care must be taken to insure that the size of a correction does not exceed the range over which the autotrack algorithm is effective. If f_1 = 2,200 MHz and f_2 = 2,258 MHz and the beam is steered to its maximum required angle off boresight ($\emptyset$ = 64.4°, θ = -22°), then α' = 33° and β' = 112° and the correction angles, from Eqs. (53) are, α_c = -1.14° and β_c = 0.30°.

A suggested tracking strategy which has considerable merit uses the following approach: The RV is tracked at f_1 after initial acquisition, and since link margin is high above ~30 km, before plasma losses become large, no correction for dual link optimization is used and f_1 is received with optimum gain. When plasma losses become significant and link margins become low, the beam is steered along an extrapolated track based on the pre-plasma track data and/or stored trajectories modified by the pre-plasma track data, and the beam offsets of Eqs. (53) are employed when in this mode to

optimize the dual link gain. The required corrections can be readily implemented in the beam steering or tracking computer. Following the period of large plasma losses, the autotracking function may be reactivated and the optimization correction removed, since link margin will be large once again. Coast mode would be activated again just one or two seconds prior to splashdown to preclude multipath degradation of the tracker.